



**HAL**  
open science

## Operando analysis of lithium profiles in Li-ion batteries using nuclear microanalysis

S. Surble, C. Paireau, J.-F. Martin, V. Tarnopolskiy, M. Gauthier, H. Khodja,  
Laurent Daniel, S. Patoux

► **To cite this version:**

S. Surble, C. Paireau, J.-F. Martin, V. Tarnopolskiy, M. Gauthier, et al.. Operando analysis of lithium profiles in Li-ion batteries using nuclear microanalysis. *Journal of Power Sources*, In press, 393, pp.37 - 42. 10.1016/j.jpowsour.2018.05.027 . cea-01790261

**HAL Id: cea-01790261**

**<https://cea.hal.science/cea-01790261>**

Submitted on 11 May 2018

**HAL** is a multi-disciplinary open access archive for the deposit and dissemination of scientific research documents, whether they are published or not. The documents may come from teaching and research institutions in France or abroad, or from public or private research centers.

L'archive ouverte pluridisciplinaire **HAL**, est destinée au dépôt et à la diffusion de documents scientifiques de niveau recherche, publiés ou non, émanant des établissements d'enseignement et de recherche français ou étrangers, des laboratoires publics ou privés.

## **Operando analysis of lithium profiles in Li-ion batteries using nuclear microanalysis**

S. Surblé<sup>a,\*</sup>, C. Paireau<sup>a</sup>, J-F. Martin<sup>b</sup>, V. Tarnopolskiy<sup>b</sup>, M. Gauthier<sup>a</sup>, H. Khodja<sup>a</sup>, L. Daniel<sup>b</sup>, S. Patoux<sup>b</sup>

a LEEL, NIMBE, CEA, CNRS, Université Paris-Saclay, CEA Saclay 91191 Gif-sur-Yvette France

b CEA / LITEN / DEHT / L2MB, 17 rue des Martyrs 38054 Grenoble cedex 9, France

---

### **HIGHLIGHT**

- *Operando* observation of lithium and fluorine concentrations and distributions in lithium-ion battery
- Direct visualization and characterization of the electrode/electrolyte interface
- Elemental characterization of LiFePO<sub>4</sub> electrodes
- Development of an *in situ* or *operando* electrochemical cell for profiling lithium using Ion Beam Analysis techniques

---

### **ABSTRACT**

A wide variety of analytical methods are used for studying the behavior of lithium-ion batteries and particularly the lithium ion distribution in the electrodes. However, the development of *in situ* / *operando* techniques proved powerful to understand the mechanisms responsible for the lithium trapping and then the aging phenomenon. Herein, we report the design of an electrochemical cell to profile *operando* lithium concentration in LiFePO<sub>4</sub> electrodes using Ion Beam Analysis techniques. The specificity of the cell resides in its ability to not only provide qualitative information about the elements present but above all to measure quantitatively their content in the electrode at different states of charge of the battery. The nuclear methods give direct information about the degradation of the electrolyte and particularly reveal inhomogeneous distributions of lithium and fluorine along the entire thickness of the electrode. Higher concentrations of fluorine is detected near the electrode/electrolyte interface while a depletion of lithium is observed near the current collector at high states of charge.

---

**Keywords** : *in situ* / *operando* analysis, nuclear microprobe, lithium-ion batteries

## 1. Introduction

1 Energy storage will be more essential in the future than it has never been in the past. Lithium-ion  
2 technology holds in this area a prominent place on the market for stationary and mobile applications.  
3  
4 Nevertheless, its specific capacity and energy density seem to reach their limits and could be  
5  
6 insufficient for the long-term. It is first thus essential to understand the aging phenomena in the  
7  
8 existing technology in order to improve their electrochemical performance with new electrode /  
9  
10 electrolyte materials or to guide future research. Different physical and chemical processes, such as  
11  
12 volume changes, phase transitions, side reactions, *etc.* mainly govern the decrease in performance of  
13  
14 a lithium-ion battery. The ageing phenomena are highly complicated to characterize. [1] *In situ* /  
15  
16 *operando* measurements allow live monitoring of these phenomena that can be directly link with the  
17  
18 battery electrochemical performance. Major developments of characterization techniques have taken  
19  
20 place in the last decade, particularly in the cell design and the electrochemical setups that are  
21  
22 compatible with the applied technique. Hark *et al.* have reviewed the recent development in *in situ*  
23  
24 methods for lithium-ion battery research. [2] However, the electrochemical community needs more *in*  
25  
26 *situ* / *operando* techniques in order to completely understand the aging mechanism involved during the  
27  
28 battery operation. Particularly, the development of techniques that enable spatial resolved  
29  
30 measurements such as *in situ* TEM and *in situ* X-ray tomography are necessary. [3–5]  
31  
32  
33

34 The Ion Beam Analysis (IBA) techniques are powerful tools to investigate in a non-invasive way  
35  
36 the elemental distributions and the composition of a material. To this purpose, the object to be  
37  
38 analyzed is probed by a beam of accelerated particles. The interactions of the beam particles with the  
39  
40 atoms of the target material induce reaction products (X-rays,  $\gamma$ -rays, charged particles), having an  
41  
42 energy characteristic of the emitting atom, including light ions such as lithium. The IBA techniques are  
43  
44 based on the detection and the analysis of these emitted radiations. Depending on the nature of the  
45  
46 detector used, several techniques are available. It is then possible to determine atomic concentration  
47  
48 from matrix elements (stoichiometry), in one dimension (depth profiles) or two dimensions (elemental  
49  
50 maps). Due to the good sensitivity to the whole periodic table, the IBA techniques have a special  
51  
52 impact on materials science and solid-state chemistry physics. However, their application to the  
53  
54 characterization of lithium-ion batteries is scarcely known and not enough developed. Only few works  
55  
56 have been devoted to this topic.  
57  
58  
59  
60  
61  
62  
63  
64  
65

1 Tadić *et al.* [6] were the first to apply IBA techniques to study the gel-polymer interfaces with Li  
2 anode and spinel cathode for Li-ion battery. The elemental composition was determined in some  
3 intercalation compounds or thin films before and after lithium insertion. [7–9] Several authors have  
4 measured the lithium extraction in cathode materials but only by chemical delithiation. [10,11]  
5 Recently, Gonzalez-Arrabal *et al.* showed that the lithium distribution in lithium-ion battery is  
6 dependent of electrode thickness. [12,13] Habrioux *et al.* carried out *ex situ* experiments on C-  
7 LiFePO<sub>4</sub> electrodes at different state of charge (SOC). [14] All of these works prove the potential of  
8 nuclear analysis techniques, especially in studying elemental concentration distributions of each  
9 element present in the target with good lateral resolution (in the μm range). More recently, Mima *et al.*  
10 perform *in situ* measurement using X-rays and γ-rays emissions.[15] Two dimensional maps of the  
11 lithium and the iron distributions were obtained in the LiFePO<sub>4</sub> electrode and the interface between the  
12 electrode and the liquid electrolyte. However, they only obtained qualitative elemental maps by  
13 combining these two IBA-techniques, no information on the whole elements presents in the electrode  
14 or at the interface was shown. On the contrary we report here a specific electrochemical cell which  
15 maps *operando* elemental concentration in a lithium-ion battery using micro-Ion Beam Analysis. The  
16 design of our cell allows the quantitative determination of the content of all elements present in a  
17 LiFePO<sub>4</sub> electrode upon charging. Especially, the distribution and concentration of light elements such  
18 as lithium and fluorine are presented as function of the state of charge of the LiFePO<sub>4</sub> electrode.  
19  
20  
21  
22  
23  
24  
25  
26  
27  
28  
29  
30  
31  
32  
33  
34  
35  
36  
37

## 38 2. Experimental section

### 39 2.1. Materials preparation

40 The positive electrode was prepared by coating an Al current collector with a slurry composed of  
41 92 wt.% of carbon-coated LiFePO<sub>4</sub> (C- LiFePO<sub>4</sub>), 4 wt.% of carbon black and 4 wt.% of CarboxyMethyl  
42 Cellulose (CMC). The negative electrode was obtained by the same process on a Cu collector with  
43 graphite as the active material. Celgard®2400 polypropylene, a Viledon polypropylene foil and 1 M  
44 LiPF<sub>6</sub> dissolved in 1:1 ethylene carbonate / diethylcarbonate (EC/DEC) were respectively used as  
45 separator and electrolyte.  
46  
47  
48  
49  
50  
51  
52  
53

### 54 2.2. Experimental procedures

55 The experimental setup and the designed electrochemical cell for *in situ* / *operando*  
56 measurements using ion beam techniques are represented on Fig.1. The experiments were carried  
57  
58  
59  
60  
61  
62  
63  
64  
65

1 out at the nuclear microprobe of the CEA - Paris Saclay. [16] The analysis chamber offers a large  
2 range of analysis techniques, which are explained in the [section 2.2.1](#). A 4-axis micron-level  
3 goniometer provides precise positioning of the samples. Two cameras visualize the sample. The first  
4 one is used to get an overview of the sample, while the second is connected to a 400 × confocal  
5 optical microscope and gives more precision on the positioning.  
6  
7

### 8 *2.2.1. Underlying principle of ion beam techniques*

9  
10 Depending on which detectors are placed in the analysis chamber, several IBA methods are  
11 available to determine simultaneously the elemental depth profiles or maps. The most common  
12 method concerns the detection of the energy of backscattered particles: the Rutherford Back-  
13 Scattering (RBS) for the heavy elements or the Particle Enhanced Scattering (PES) for the lightest  
14 ones (with the proton beam). Nuclear reactions also occur with light elements, giving rise to the NRA  
15 technique (Nuclear Reaction Analysis) which signal adds up to the RBS / PES one. Back-scattering  
16 analysis provides the ability to distinguish the atomic masses of elements and their distribution in  
17 depth as a function of the detected energy. The others methods are based on the detection of X-rays  
18 and  $\gamma$ -rays emissions (respectively PIXE and PIGE for Particle Induced X-ray or  $\gamma$ -ray Emission). The  
19 PIXE method is directly comparable with electron probe microanalysis (EPMA) with very similar  
20 spectra, except that there is negligible primary bremsstrahlung background due to the much higher  
21 particle mass. Consequently, trace element analysis using PIXE has a detection limit orders of  
22 magnitude lower than what can be attainable by X-rays spectrometry techniques using electron  
23 excitation. As for the PIXE method, where each element has a characteristic X-rays energy, the  
24 energy of the  $\gamma$ -emitted during the irradiation is characteristic of one element for the PIGE technique.  
25  
26

27 Protons beams in the range 1.0 - 4.0 MeV are preferred for lithium and fluorine analysis, as it offers an  
28 optimal compromise of probing techniques, listed hereafter:  
29

- 30 - Efficient and well-known EBS cross sections of all elements
- 31 - Enhanced PIXE cross sections (compared to other projectiles)
- 32 - Available NRA and PIGE reactions for both Li and F.

33  
34 Regarding Li and F measurements, PIGE technique was selected as it produces well separated  
35 spectrum contributions (478keV and 197 keV  $\gamma$ -rays from  ${}^7\text{Li}(p,p'\gamma){}^7\text{Li}$  and  ${}^{19}\text{F}(p,p'\gamma){}^{16}\text{O}$  reactions  
36 respectively), while NRA gives rise to very close Li and F contributions (7471.4keV and 7561.4keV  $\alpha$   
37 particles from  ${}^7\text{Li}(p, \alpha_0){}^4\text{He}$  and the  ${}^{19}\text{F}(p, \alpha_0){}^{16}\text{O}$  reactions respectively). Although the RBS and PIXE  
38  
39  
40  
41  
42  
43  
44  
45  
46  
47  
48  
49  
50  
51  
52  
53  
54  
55  
56  
57  
58  
59  
60  
61  
62  
63  
64  
65

spectra are not directly used for the lithium content determination, these techniques provide information about all elements present on the analyzed target.

### 2.2.2. Specific consideration for *in situ* cell design

Many groups have designed electrochemical cells for *in situ* or *operando* measurements. *In situ* cells have not a single ideal design. Indeed, each cell needs to fit the experimental setup available for the experiment purpose. In this paper, we present the electrochemical cell that we develop with specific requirements for IBA experiments:

- Being able to cycle electrochemically for ten cycles at different rate of charge (from C/5 to C/100).
- Being airtight. IBA techniques are generally performed under vacuum while the charge / discharge of a Li-ion battery is achieved under inert atmosphere.
- Taking account of the geometric space of the analysis chamber.
- Providing a good quality of IBA spectra in 30 minutes or less with no contributions apart from those of the electrodes / electrolyte materials.

To conduct ion beam measurements on an operating battery, a transparent window needs to be incorporated to the design in order to allow the ion beam to reach the electrode(s) / electrolyte under investigation. Since the interaction between the beam and the window can induce an undesirable background, the exit window must fulfill the following conditions: (i) minimum of energy loss and energy straggling; (ii) minimum of interfering signal; (iii) good resistance to pressure and irradiation. As silicon nitride windows are commonly used to extract ion beam to air, we choose for our electrochemical cell a 200 nm Si<sub>3</sub>N<sub>4</sub> window.

The analysis chamber is usually equipped with three detectors, recording simultaneously the backscattered particles, X-ray and  $\gamma$ -ray emissions. We choose to exploit with our electrochemical cell the backscattered particles (RBS) and the  $\gamma$ -ray emissions (PIGE) as explained in section 2.2.1. In the present work, the measurements with the nuclear microprobe have been performed using a 3×3  $\mu\text{m}^2$  proton beam of 2.6 MeV. The battery is assembled inside a glove-box using the order described in [Fig.](#)

1. Stainless steel discs and spring ensured pressure in the system and good electrical contact between the battery components.

## 3. Results and discussion

### 3.1. Preliminary tests

A series of tests were made for evaluating the cell and the reliability of the electrochemical data.

1  
2 **Fig. 2** shows the cycling performance at C/10 rate between 2.5V and 3.8V for the LiFePO<sub>4</sub> / Graphite  
3 battery assembled in a Swagelok cell and in the *in situ* electrochemical cell. The initial capacity is  
4 similar (near 140 mA.h.g<sup>-1</sup>) in both setups (using a different quantity of electrolyte) but the polarization  
5 is higher with the *in situ* cell. The irreversible capacity is identical for the battery cycled with few drops  
6 of electrolyte for the first cycle. The higher capacity fading of the *in situ* cell, observed after 10 cycles,  
7 is ascribed to a loss of pressure and electrical contact between electrodes and current collectors in the  
8 cell. The electrochemical cell designed to perform *in situ* or *operando* nuclear experiments delivers  
9 electrochemical performances comparable to those obtained with classical electrochemical cells on  
10 the first two cycles.  
11  
12  
13  
14  
15  
16  
17  
18

### 19 3.2. Lithium and fluorine profiles

20  
21  
22 Elemental or full concentration maps can be drawn from specific region of interest. As shown in  
23 **Fig. 3**, each component of the battery are clearly identified in the map drawn from the RBS spectrum  
24 (1000-3000 keV).  
25  
26  
27

28 **Fig. 4** shows typical RBS and PIGE spectra corresponding to the region of the LiFePO<sub>4</sub> material /  
29 electrolyte in the *in situ* cell. RBS technique is based on the fact that the energy of a backscattered  
30 particle depends both on the mass of the target atom (kinematic factor) and the depth at which the  
31 scattering took place (energy loss on the way to and from the point of interaction). This allows to  
32 profile the elemental composition of the sample close to the surface (see [suppl. info. Fig. S1](#)). A RBS  
33 spectrum is composed of a succession of narrow peaks for a thin film and steps for a thicker target. In  
34 our work, the simulation of the RBS spectra is performed using several layers representing the  
35 different elements or components the beam is meeting. The ion beam meets first the Si<sub>3</sub>N<sub>4</sub> window,  
36 then the argon layer, located in the interspace between the window and the battery, and finally the  
37 LiFePO<sub>4</sub> electrode. The presence of argon events on the RBS spectrum arises from the gas  
38 encapsulated in the *in situ* cell, as the battery is assembled in an argon glove box to avoid any  
39 possible reaction with moisture or air. If a decomposition of the electrode or electrolyte should happen,  
40 supplementary layers with others compositions will arised on the spectrum. Following the numbers of  
41 observed layers and its thickness, the detected energy for one element is shifted towards lower energy  
42 (compared to the surface energy position).  
43  
44  
45  
46  
47  
48  
49  
50  
51  
52  
53  
54  
55  
56  
57  
58  
59  
60  
61  
62  
63  
64  
65

As described elsewhere [14,17], the fluorine and lithium concentrations are determined in PIGE analysis by comparison with reference samples using the following relation:

$$\frac{[X_{sample}]}{[X_{standard}]} = \frac{S_{sample}}{S_{standard}} \times \frac{A_{sample}}{A_{standard}} \times \frac{N_{\omega standard}}{N_{\omega sample}}$$

where S is the stopping power of the sample, A the peak area associated with  $\gamma$  -ray transitions observed for an element X (F at 197 keV and Li at 478 keV) and  $N_{\omega}$  the number of protons per solid angle unit delivered to the selected area. The reference samples are respectively  $\text{CaF}_2$  glass and pristine  $\text{LiFePO}_4$  electrode. The composition of this electrode is verified using the NIST Silicate Glass Certified Reference Material SRM 610 (428 ppm). Using SIMNRA<sup>®</sup> software [18], simulations of the RBS spectra as function of the composition of the target give access to the values of S and  $N_{\omega}$ . The whole process is repeated before reaching a global coherency.

First, only the three layers mentioned above ( $\text{Si}_3\text{N}_4$ , Ar and electrode) are used for the simulation of the RBS spectra before charging the battery (Fig. 4a). When the charge of the battery occurs, others layers need to be added. The energy of a backscattered particle is now spread over several keV (Fig. 4b). This modification seems to be induced by a degradation of the electrolyte. We note that the regions corresponding to fluorine and phosphorus atoms (respectively near 2122 keV and 2302 keV), are no more composed of two distinguishing steps but successive narrow steps. Moreover, the Ar signal decreases during the charge. Yoshida *et al.* [19] have studied the degradation mechanism of alkyl carbonate solvents used in lithium-ion cells during initial charging. The electrolyte degradation produces essentially gases such as  $\text{H}_2$ ,  $\text{CH}_4$ ,  $\text{C}_2\text{H}_4$ ,  $\text{CO}$  and  $\text{CO}_2$ . [20] The simulation of the RBS spectra is then performed by adding C, O, H and F in the layer containing the argon. The initial Ar signal is thus hidden by the presence of other gases. As a result the simulation of the *in situ* RBS spectra is particularly hard to perform due to the presence of multiple layers and to the permanent change of the electrolyte composition. Although it is not possible to estimate with a good accuracy the full composition of each layer, the stopping power of the last layer (corresponding to the electrode) does not change drastically (2-3% of change), and the concentration of lithium and fluorine can thus be estimated from the PIGE spectra with a good accuracy. In this case, the intensities of the  $^{19}\text{F}(p,p'\gamma)^{16}\text{O}$  at 197keV and the  $^7\text{Li}(p,p'\gamma)^7\text{Li}$  reaction at 478keV are directly proportional to the concentration. The lithium content decreases as a function of the state of charge (as expected) while the fluorine content changes randomly (Fig. 4c).

1  
2  
3  
4  
5  
6  
7  
8  
9  
10  
11  
12  
13  
14  
15  
16  
17  
18  
19  
20  
21  
22  
23  
24  
25  
26  
27  
28  
29  
30  
31  
32  
33  
34  
35  
36  
37  
38  
39  
40  
41  
42  
43  
44  
45  
46  
47  
48  
49  
50  
51  
52  
53  
54  
55  
56  
57  
58  
59  
60  
61  
62  
63  
64  
65

Fig. 5 displays the composition of the electrode from the current collector to the electrolyte at different steps during the charge (*i.e.* SOC). Elemental maps of lithium and fluorine are extracted from the PIGE spectra. The composition of the electrode close to the interface of the electrode / liquid electrolyte is not constant during the charge of the battery. Unfortunately, **the different contributions of lithium present in the sample (inside the electrode or in the electrolyte) cannot be deciphered using any hypothesis, only the whole elemental lithium concentration and distribution are available.**

The lithium and fluorine distributions are extracted from the elemental maps drawn from the  $\gamma$ -rays at 478keV and 197keV respectively. We observe systematically a higher concentration of fluorine near the electrode / electrolyte interface. On the other hand, the lithium distribution as a function of the SOC seems to be smoother along the cross section (from the current collector to the electrolyte interface), suggesting a homogeneous diffusion of lithium throughout the entire thickness of the electrode. However, for the 80% and 88% SOC, less lithium is found near the current collector, denoting some lithium diffusion hindrance at the end of charge. The Li and F distributions reveal that electrochemical reactions occurs, that forms passivation layer (initial electrode thickness 160 $\mu$ m).

In order to estimate the ratio of electrode / electrolyte, we use the proportion of the pristine delithiated composite electrode. In all experiments, we scan the beam on selected areas of the sample (from 30  $\times$  180  $\mu$ m<sup>2</sup>). We consider that all iron are included in delithiated electrode and thus do not participate in a passivation layer. We deduce that the analyzed region contains around 92.5  $\pm$  0.3 at. % of electrolyte (LiPF<sub>6</sub> in DEC/EC) and degradation products and 5.2  $\pm$  0.6 at. % of delithiated composite electrode (included FePO<sub>4</sub>, CMC and C fibers). This composition remains in the same order for all analyzed SOCs. Numerous electrochemical or chemical reactions occur during the battery operation due to electrolyte degradation, giving rise to different compounds, leading to the observed. The heterogeneity observed here at the electrode / electrolyte interface through the presence of C, O, H and F in the interspace between the Si<sub>3</sub>N<sub>4</sub> layer and the battery is due to the presence of electrolyte and to these electrolyte degradation reactions.

Although few drops of liquid electrolyte are used in the cell and the ion beam analysis is performed essentially on the positive electrode (with small contribution of parts of the current collector and liquid electrolyte), we analyze essentially the electrolyte and its decomposition products. The main problem is that liquid flows in the space between the window and the battery. Using less electrolyte led to a

1 short circuit of the battery. The obtained spectra are thus more complicated to exploit, but the results  
2 provide valuable information on the lithium distribution.

#### 3 4 **4. Conclusion**

5 We presented *operando* RBS and PIGE measurements applied to measure the lithium and the  
6 fluorine distributions in a lithium-ion cell with a LiFePO<sub>4</sub> electrode. To this end, we designed a special  
7 electrochemical cell allowing for the first time qualitative and quantitative analysis of all the elements in  
8 the electrode using IBA techniques. The cell is able to deliver electrochemical performances  
9 comparable to those obtained with classical electrochemical cells on the first two cycles. The  
10 elemental maps, drawn using the  ${}^7\text{Li}(p,p'\gamma){}^7\text{Li}$  and the  ${}^{19}\text{F}(p,p'\gamma){}^{16}\text{O}$  reactions of the PIGE spectra,  
11 show an inhomogeneity of their distributions with a higher concentration of fluorine near the  
12 electrode/electrolyte interface and a depletion of lithium near the current collector at high state of  
13 charge. The use of a liquid electrolyte creates complications for the analyses: electrode contributions  
14 to the spectra is only 5% as the liquid flows in the space between the battery and the Si<sub>3</sub>N<sub>4</sub> window,  
15 rendering the interpretation of results difficult. The use of solid electrolyte in all solid-state batteries  
16 should give more information about the parasite electrochemical reaction (composition and thickness).  
17 In summary, we have demonstrated how powerful ion beam techniques can be for investigating the  
18 lithium profile in lithium batteries. Interestingly, the distribution of others elements such as sodium or  
19 magnesium is also possible using the reaction  ${}^{23}\text{Na}(p,p'\gamma){}^{23}\text{Na}$  at 439 keV or  ${}^{24}\text{Mg}(p,p'\gamma){}^{24}\text{Mg}$  at 1368  
20 keV [21,22] and is believed to be of great interest for studying reaction and degradation mechanisms  
21 in Na-ion and Mg-ion batteries.

#### 22 **Acknowledgments**

23 This work is supported by the NTE (Nouvelles Technologies de l'Energie) program of the CEA. We  
24 would like to acknowledge Jim Hoarau for the design of the electrochemical cell and helpful discussions,  
25 and Didier Guillier and Yvan Kilisky for accelerator operation.

#### 26 27 28 29 30 31 32 33 34 35 36 37 38 39 40 41 **References**

- 42  
43  
44  
45  
46  
47  
48  
49  
50  
51  
52  
53  
54 [1] A. Barré, B. Deguilhem, S. Grolleau, M. Gérard, F. Suard, D. Riu, A review on lithium-ion battery  
55 ageing mechanisms and estimations for automotive applications, J. Power Sources. 241 (2013)  
56 680–689.  
57 [2] P.P.R.M.L. Harks, F.M. Mulder, P.H.L. Notten, In situ methods for Li-ion battery research: A  
58 review of recent developments, J. Power Sources. 288 (2015) 92–105.  
59  
60  
61  
62  
63  
64  
65

- 1  
2  
3  
4  
5  
6  
7  
8  
9  
10  
11  
12  
13  
14  
15  
16  
17  
18  
19  
20  
21  
22  
23  
24  
25  
26  
27  
28  
29  
30  
31  
32  
33  
34  
35  
36  
37  
38  
39  
40  
41  
42  
43  
44  
45  
46  
47  
48  
49  
50  
51  
52  
53  
54  
55  
56  
57  
58  
59  
60  
61  
62  
63  
64  
65
- [3] F. Sun, H. Markötter, K. Dong, I. Manke, A. Hilger, N. Kardjilov, J. Banhart, Investigation of failure mechanisms in silicon based half cells during the first cycle by micro X-ray tomography and radiography, *J. Power Sources*. 321 (2016) 174–184.
  - [4] C.-Y. Chen, T. Sano, T. Tsuda, K. Ui, Y. Oshima, M. Yamagata, M. Ishikawa, M. Haruta, T. Doi, M. Inaba, S. Kuwabata, In situ Scanning Electron Microscopy of Silicon Anode Reactions in Lithium-Ion Batteries during Charge/Discharge Processes, *Sci. Rep.* 6 (2016).
  - [5] C.P. Grey, J.M. Tarascon, Sustainability and in situ monitoring in battery development, *Nat. Mater.* 16 (2017) 45–56.
  - [6] T. Tadić, M. Jakšić, Z. Medunić, E. Quartarone, P. Mustarelli, Microbeam studies of gel–polymer interfaces with Li anode and spinel cathode for Li ion battery applications using PIGE and PIXE spectroscopy, *Nucl. Instrum. Methods Phys. Res. Sect. B Beam Interact. Mater. At.* 181 (2001) 404–407.
  - [7] P. Berger, S. Pruvost, C. Hérold, P. Lagrange, Proton enhanced scattering and nuclear reaction analysis microcharacterization of ternary graphite–lithium–calcium intercalation compounds, *Nucl. Instrum. Methods Phys. Res. Sect. B Beam Interact. Mater. At.* 219–220 (2004) 1005–1009.
  - [8] J. Światowska-Mrowiecka, S. de Diesbach, V. Maurice, S. Zanna, L. Klein, E. Briand, I. Vickridge, P. Marcus, Li-Ion Intercalation in Thermal Oxide Thin Films of MoO<sub>3</sub> as Studied by XPS, RBS, and NRA, *J Phys Chem C*. 112 (2008) 1105011058.
  - [9] M.V. Reddy, B. Pecquenard, P. Vinatier, C. Wannek, A. Levasseur, P. Moretto, RBS and NRA analyses of lithium inserted amorphous Li<sub>1+x</sub>NiVO<sub>4</sub> films, *Nucl Instr Meth B*. 246 (2006) 397401.
  - [10] E. Andrade, A. Romero Núñez, A. Ibarra Palos, J. Cruz, M.F. Rocha, C. Solis, O.G. de Lucio, E.P. Zavala, Ion beam analysis of partial lithium extraction of LiMn<sub>2</sub>O<sub>4</sub> by chemical delithiation, *Nucl. Instrum. Methods Phys. Res. Sect. B Beam Interact. Mater. At.* 269 (2011) 440–443.
  - [11] M. Lachal, R. Bouchet, A. Boulineau, S. Surblé, C. Rossignol, F. Alloin, S. Obbade, Remarkable impact of grains boundaries on the chemical delithiation kinetics of LiFePO<sub>4</sub>, *Solid State Ion.* 300 (2017) 187–194.
  - [12] K. Mima, R. Gonzalez-Arrabal, H. Azuma, A. Yamazaki, C. Okuda, Y. Ukyo, H. Sawada, K. Fujita, Y. Kato, J.M. Perlado, S. Nakai, Li distribution characterization in Li-ion batteries positive electrodes containing Li<sub>x</sub>Ni<sub>0.8</sub>Co<sub>0.15</sub>Al<sub>0.05</sub>O<sub>2</sub> secondary particles ( $0.75 \leq x \leq 1.0$ ), *Nucl. Instrum. Methods Phys. Res. Sect. B Beam Interact. Mater. At.* 290 (2012) 79–84.
  - [13] R. Gonzalez-Arrabal, M. Panizo-Laiz, K. Fujita, K. Mima, A. Yamazaki, T. Kamiya, Y. Orikasa, Y. Uchimoto, H. Sawada, C. Okuda, Y. Kato, J.M. Perlado, Meso-scale characterization of lithium distribution in lithium-ion batteries using ion beam analysis techniques, *J. Power Sources*. 299 (2015) 587–595.
  - [14] A. Habrioux, S. Surblé, P. Berger, H. Khodja, A. D’Affroux, S. Mailley, T. Gutel, S. Patoux, Nuclear microanalysis of lithium dispersion in LiFePO<sub>4</sub> based cathode materials for Li-ion batteries, *Nucl. Instrum. Methods Phys. Res. Sect. B Beam Interact. Mater. At.* 290 (2012) 13–18.
  - [15] A. Yamazaki, Y. Orikasa, K. Chen, Y. Uchimoto, T. Kamiya, M. Koka, T. Satoh, K. Mima, Y. Kato, K. Fujita, In-situ measurement of the lithium distribution in Li-ion batteries using micro-IBA techniques, *Nucl. Instrum. Methods Phys. Res. Sect. B Beam Interact. Mater. At.* 371 (2016) 298–302.
  - [16] H. Khodja, E. Berthoumieux, L. Daudin, J.-P. Gallien, The Pierre Süe Laboratory nuclear microprobe as a multi-disciplinary analysis tool, *Nucl. Instrum. Methods Phys. Res. Sect. B Beam Interact. Mater. At.* 181 (2001) 83–86.
  - [17] C. Crépisson, M. Blanchard, H. Bureau, C. Sanloup, A.C. Withers, H. Khodja, S. Surblé, C. Raepsaet, K. Béneut, C. Leroy, P. Giura, E. Balan, Clumped fluoride-hydroxyl defects in forsterite: Implications for the upper-mantle, *Earth Planet. Sci. Lett.* 390 (2014) 287–295.
  - [18] M. Mayer, J.L. Duggan, B. Stippec, I.L. Morgan, SIMNRA, a simulation program for the analysis of NRA, RBS and ERDA, in: *AIP Conf. Proc.*, AIP, 1999: pp. 541–544.
  - [19] H. Yoshida, T. Fukunaga, T. Hazama, M. Terasaki, M. Mizutani, M. Yamachi, Degradation mechanism of alkyl carbonate solvents used in lithium-ion cells during initial charging, *J. Power Sources*. 68 (1997) 311–315.

- 1  
2  
3  
4  
5  
6  
7  
8  
9  
10  
11  
12  
13  
14  
15  
16  
17  
18  
19  
20  
21  
22  
23  
24  
25  
26  
27  
28  
29  
30  
31  
32  
33  
34  
35  
36  
37  
38  
39  
40  
41  
42  
43  
44  
45  
46  
47  
48  
49  
50  
51  
52  
53  
54  
55  
56  
57  
58  
59  
60  
61  
62  
63  
64  
65
- [20] K. Kumai, H. Miyashiro, Y. Kobayashi, K. Takei, R. Ishikawa, Gas generation mechanism due to electrolyte decomposition in commercial lithium-ion cell, *J. Power Sources*. 81–82 (1999) 715–719.
- [21] M. Roberge, H. Bureau, N. Bolfan-Casanova, D.J. Frost, C. Raepsaet, S. Surble, H. Khodja, A.-L. Auzende, G. Fiquet, Is the transition zone a deep reservoir for fluorine?, *Earth Planet. Sci. Lett.* 429 (2015) 25–32.
- [22] G.L.N. Reddy, S. Kumar, S.V. Kumar, J.V. Ramana, S. Veena, V.S. Raju, Depth profiling of Mg by 2010keV resonance of  $^{24}\text{Mg}(p,p'\gamma)^{24}\text{Mg}$  nuclear reaction, *Nucl. Instrum. Methods Phys. Res. Sect. B Beam Interact. Mater. At.* 266 (2008) 3281–3289.

Figure 1  
[Click here to download high resolution image](#)

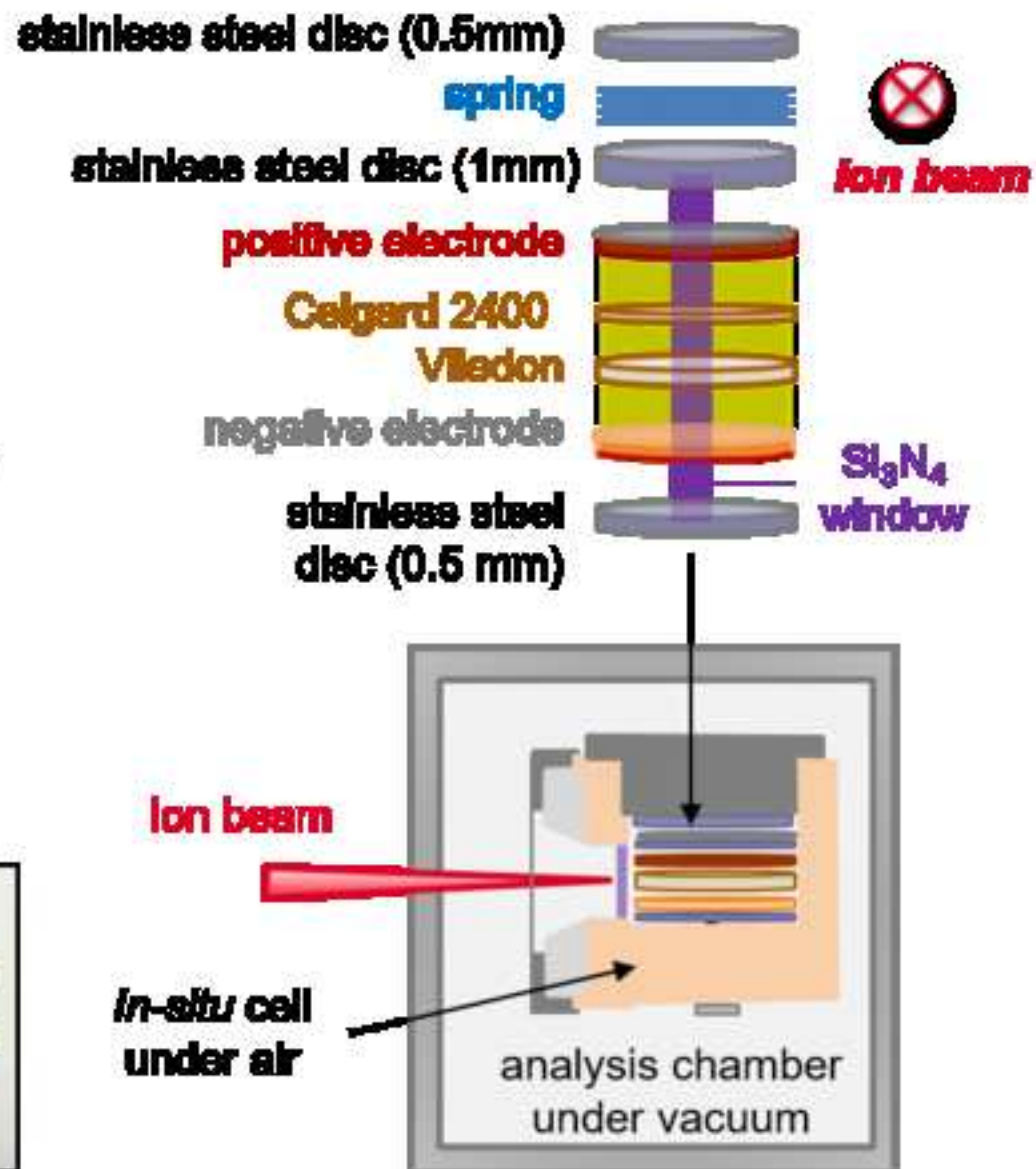
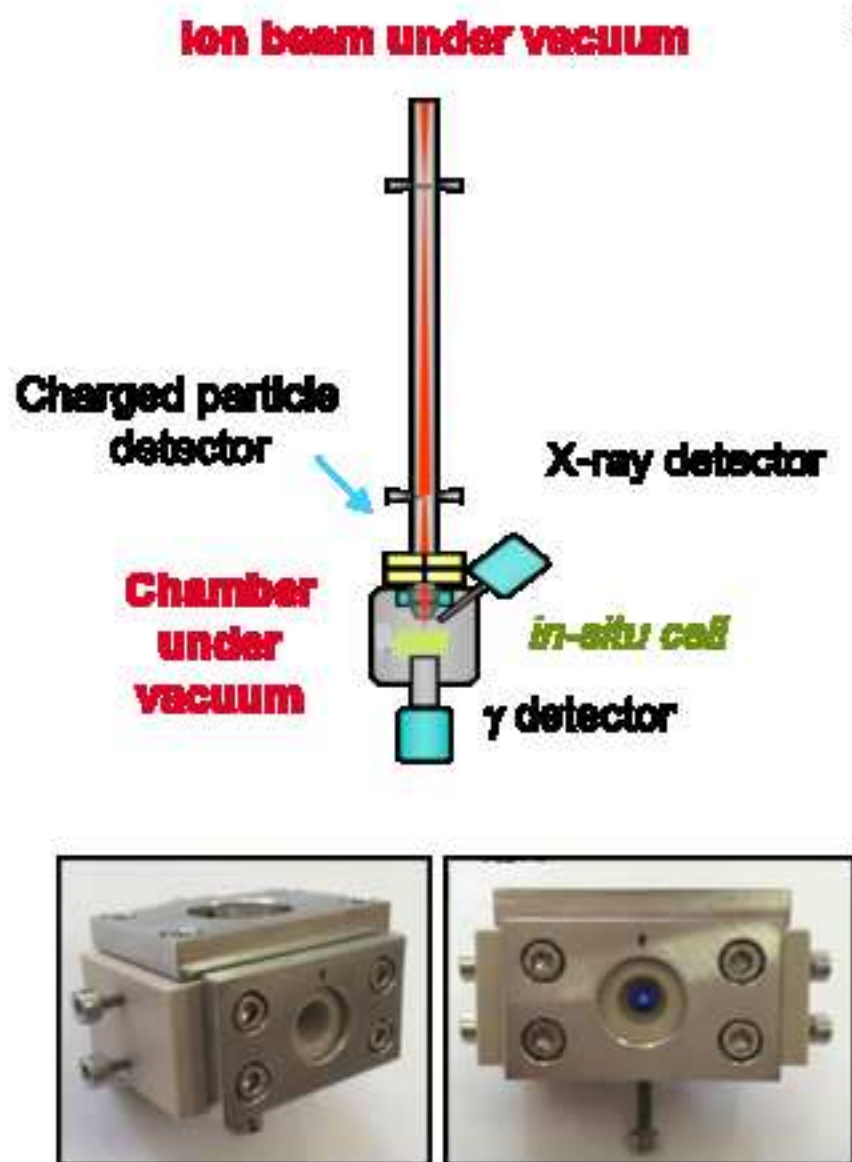


Figure 2  
[Click here to download high resolution image](#)

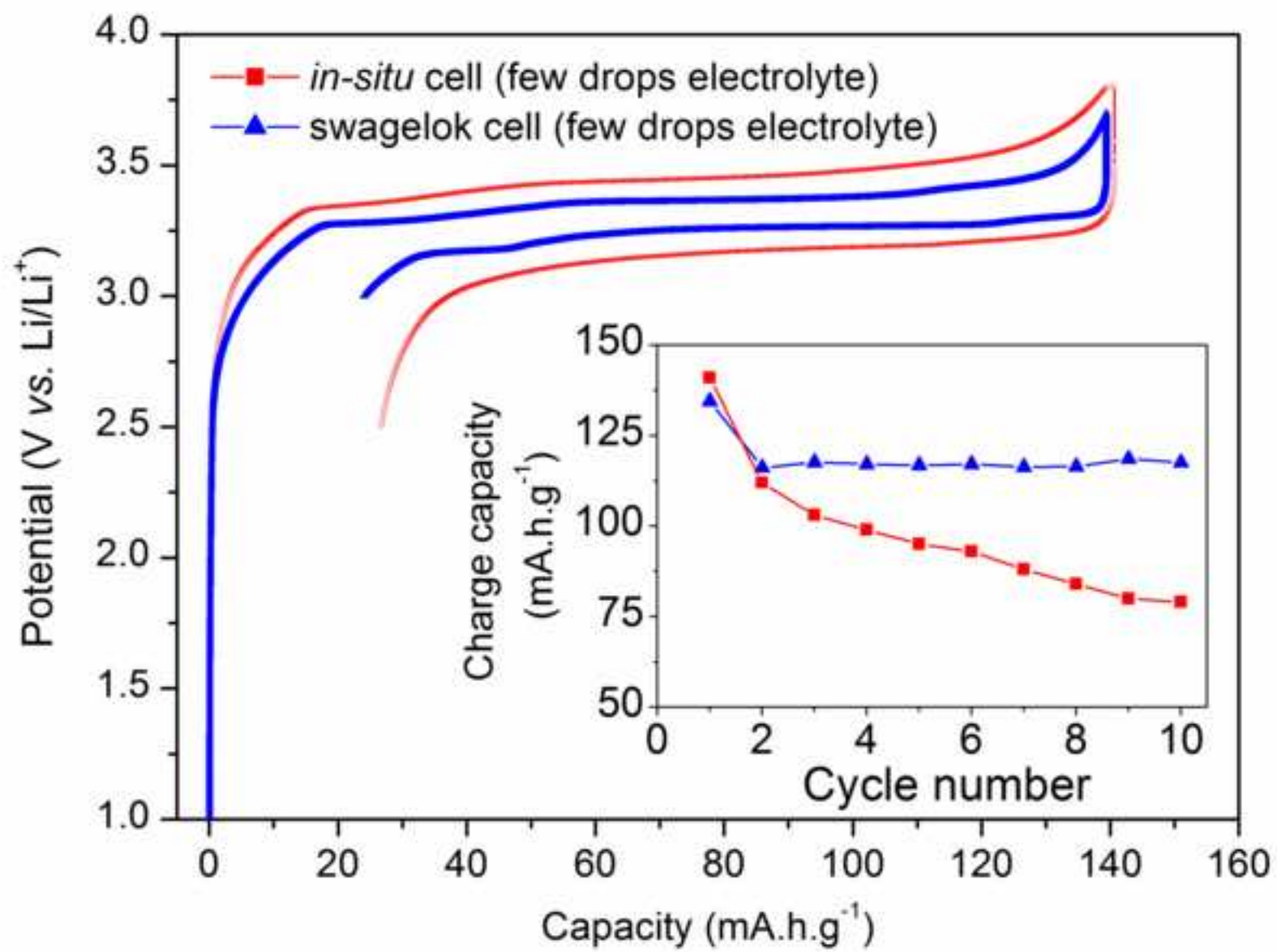


Figure 3  
[Click here to download high resolution image](#)

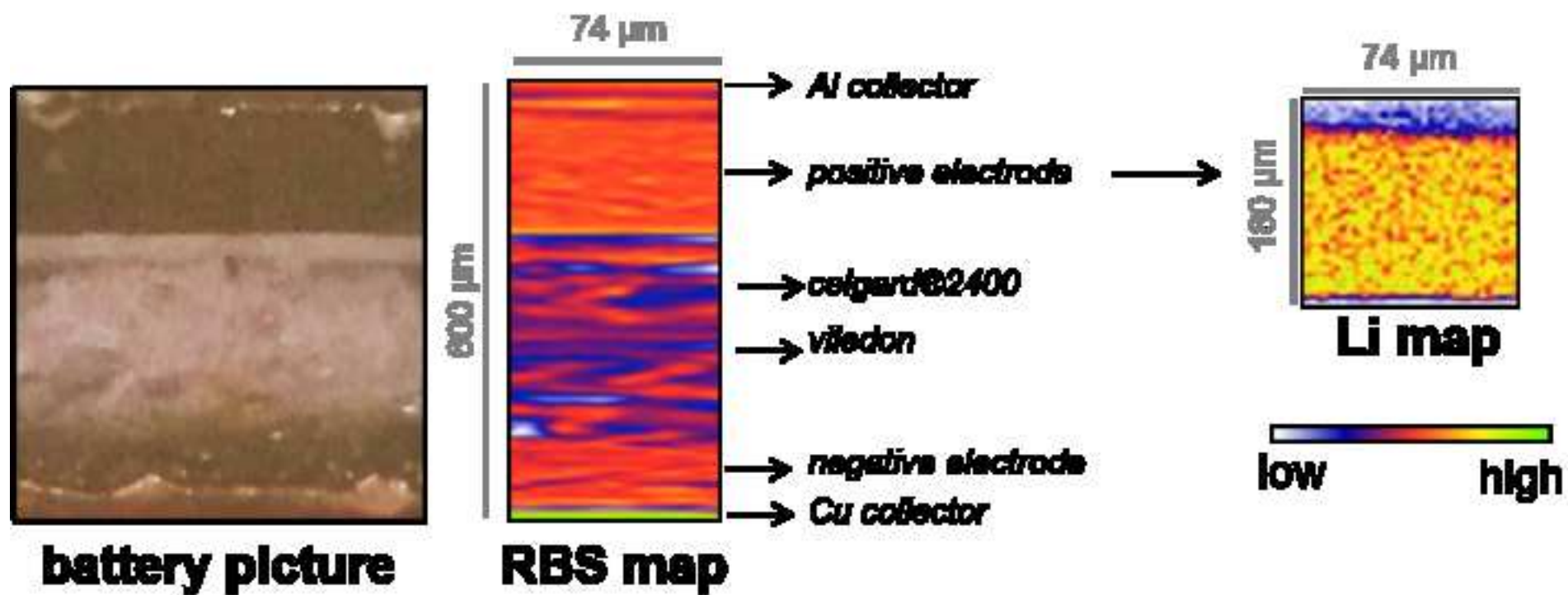


Figure 4a

[Click here to download high resolution image](#)

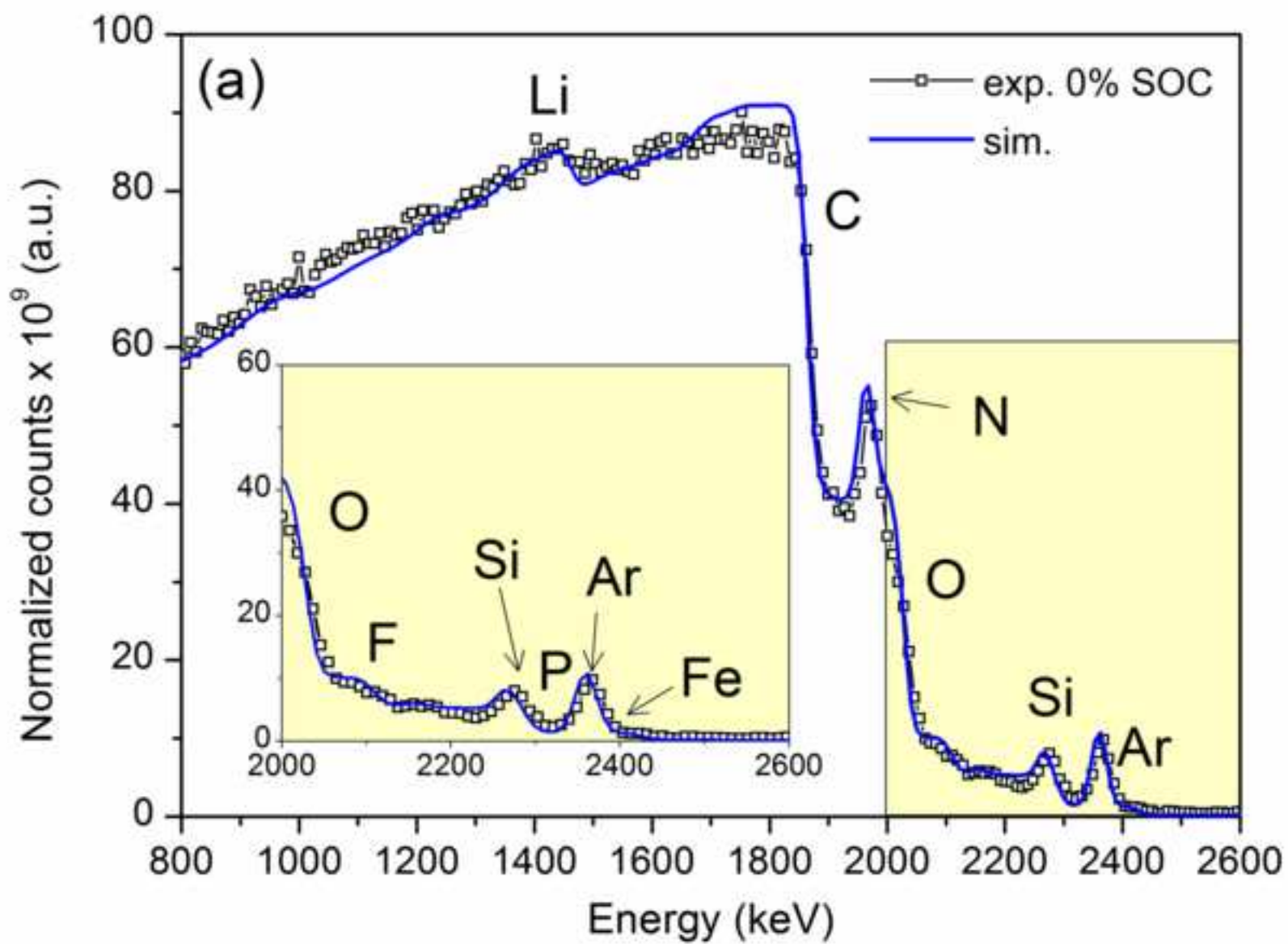


Figure 4b  
[Click here to download high resolution image](#)

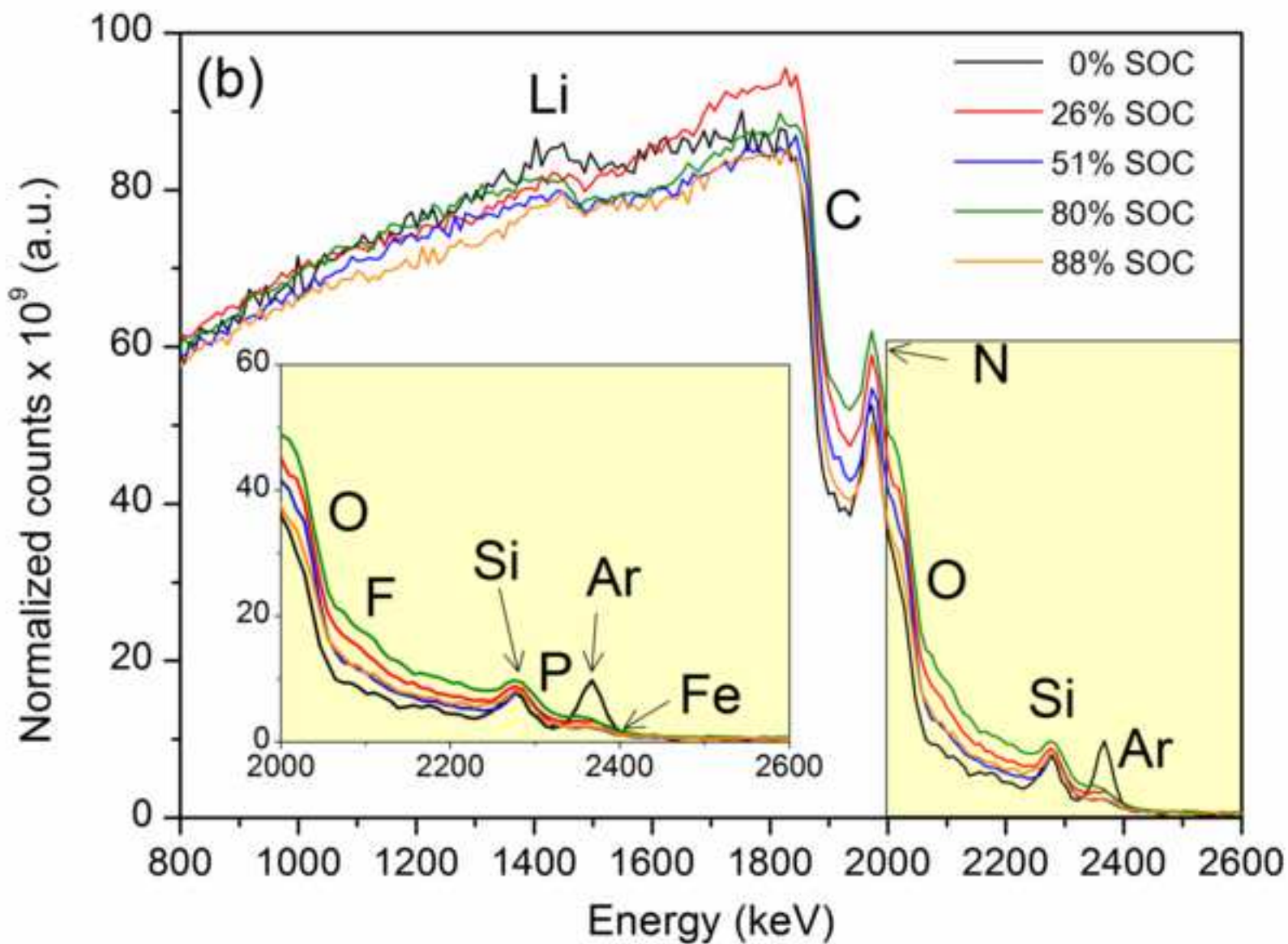


Figure 4c  
[Click here to download high resolution image](#)

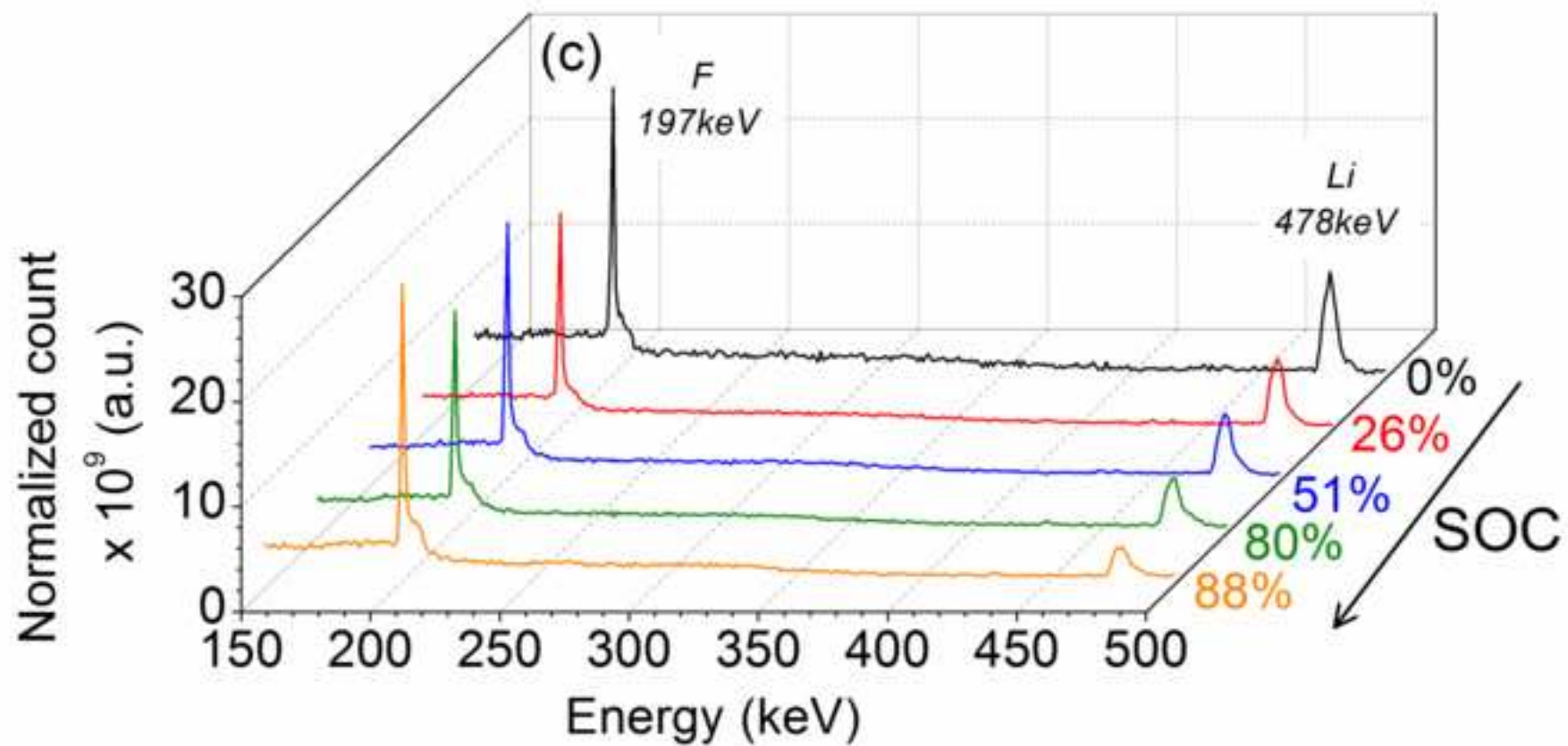


Figure 5a  
[Click here to download high resolution image](#)

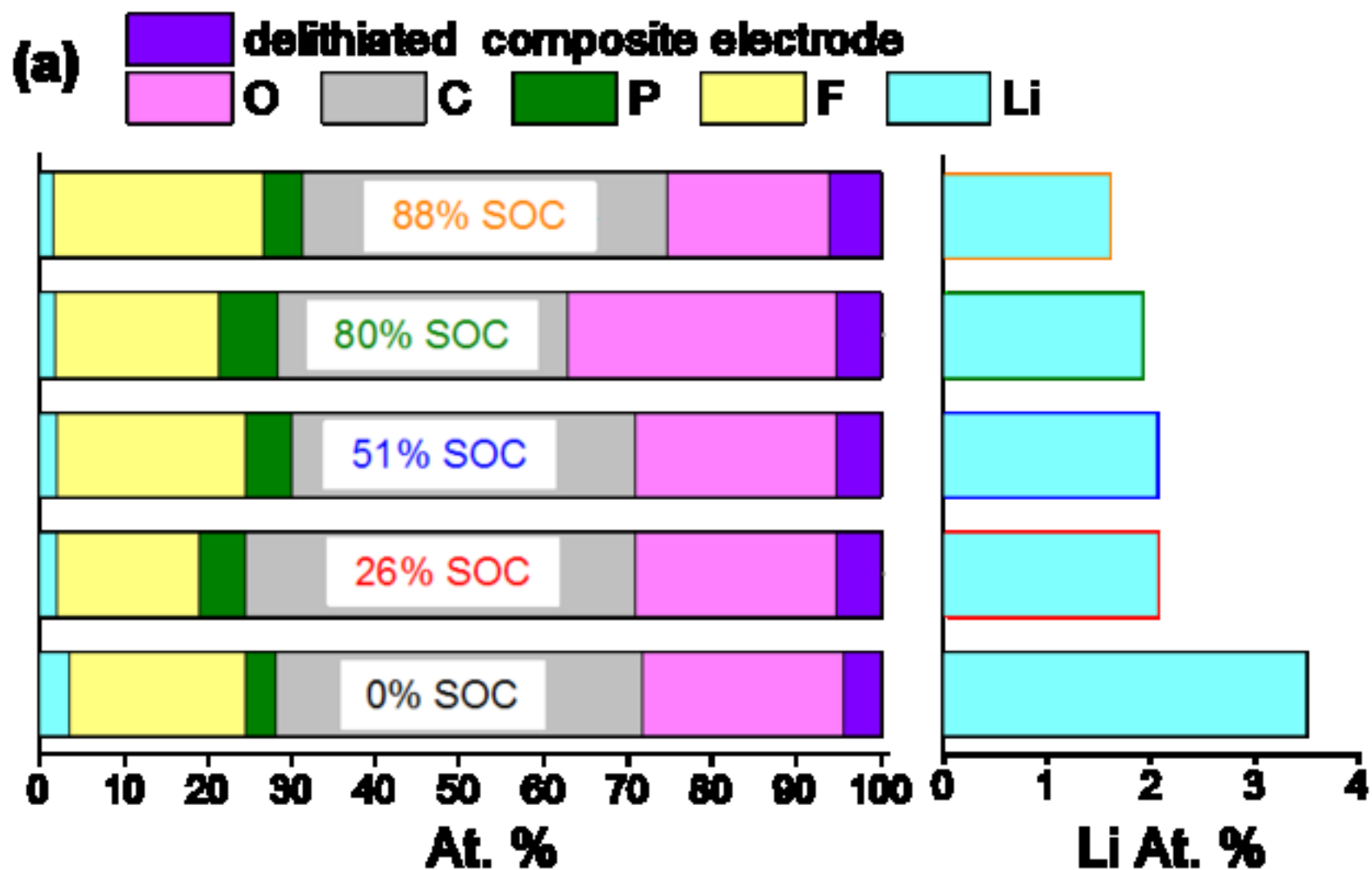


Figure 5b  
[Click here to download high resolution image](#)

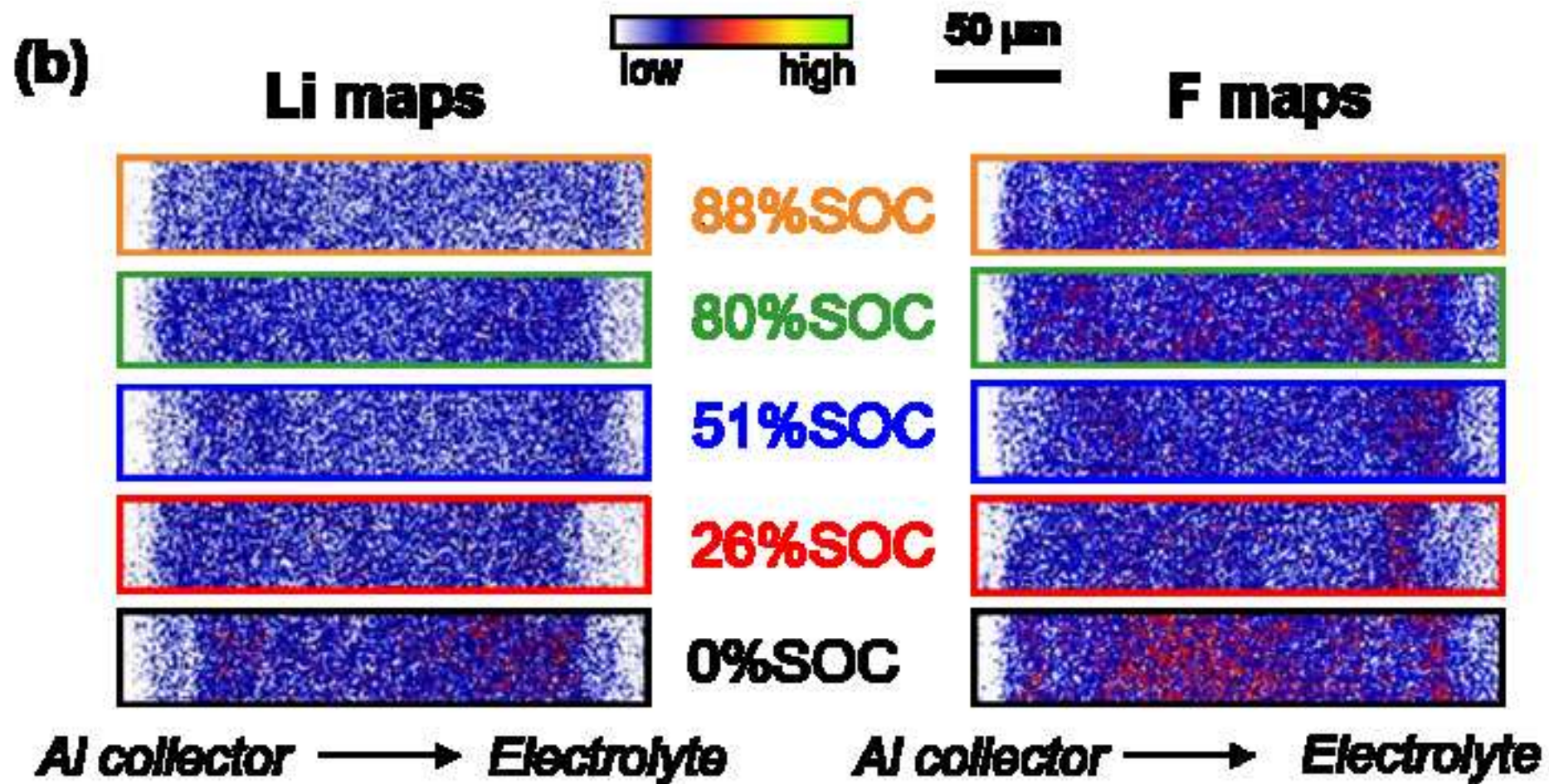
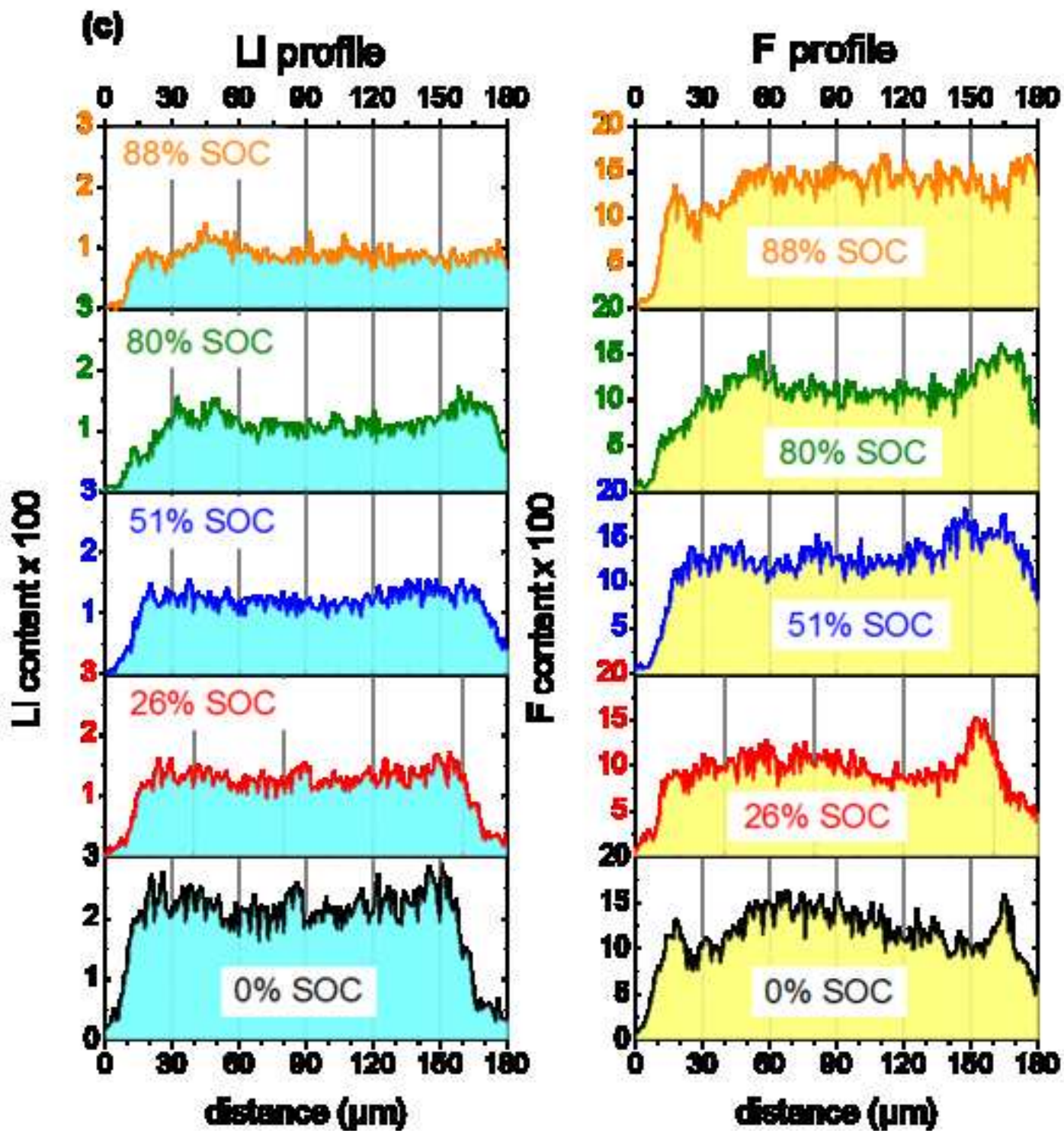


Figure 5c  
[Click here to download high resolution image](#)



## Figure captions

**Fig. 1.** Schematic illustrations of the experimental setup and the designed electrochemical cell for ion beam analysis.

**Fig. 2.** First electrochemical cycle for  $\text{LiFePO}_4$  / Graphite in Swagelok cell and in situ cell with different quantity of electrolyte. Inset shows the charge capacity vs. cycle number for a full cell assembled either in a Swagelok device or in the in situ cell with a different quantity of electrolyte.

**Fig. 3.** Identification of each component of the battery on the map drawn from the RBS spectra. The lithium map is drawn from the  ${}^7\text{Li}(p,p'\gamma){}^7\text{Li}$  reaction at 478 keV from the PIGE spectrum.

**Fig. 4. (a)** Example of the simulation of RBS spectrum for a  $\text{LiFePO}_4$  material in the in situ cell before charging. **(b)** and **(c)** Evolution of the RBS and PIGE spectra of electrode / electrolyte region during the charge of the in situ cell at C/75 rate. For the sake of comparison, each spectrum is normalized by the number of incident particles.

**Fig. 5. (a)** Elemental composition obtained using nuclear microanalysis in the cross section of the  $\text{LiFePO}_4$  electrode (from the Al collector to the electrolyte). The composition of delithiated composite electrode is estimated from the proportion of the pristine delithiated composite electrode. **(b-c)** Lithium and fluorine maps drawn from the  $\gamma$ -rays at 478 keV and 197 keV respectively and their distributions along the electrode depth (the left side of the map corresponds to the electrode on the Al collector:  $d=0\mu\text{m}$ , and the right side to the separator:  $d=180\mu\text{m}$ ) as a function of the state of charge (SOC).